RSC Advances

PAPER

View Article Online
View Journal | View Issue

Cite this: *RSC Adv.*, 2025, **15**, 44164

Photochemically-made gold nanorods for adsorption and SERS detection of cocaine and benzoylecgonine in latent fingerprints

Marco A. de Souza, *[a] Karolyne V. de Oliveira, [b] Lucas B. Pereira, [b] Marcelo H. Sousa, [c] Jez W. B. Braga [d] and Leonardo G. Paterno [d]

Received 16th June 2025
Accepted 29th October 2025

DOI: 10.1039/d5ra04284d

rsc.li/rsc-advances

Detection of illegal drugs in fingermarks is a routine activity of the scientific police and it can be better carried out with the help of more sensitive and faster analytical tools. In this regard, this contribution proposes and tests a SERS-based method for the rapid detection of cocaine hydrochloride (COC) in latent fingerprints (LFP) using photochemically-made CTAB-coated gold nanorods (AuNRs) as SERS-active substrates. As a key point, removal of excessive CTAB from the AuNR colloids is essential to achieve the largest Raman signal enhancement. The method is capable of detecting COC in dried solutions (~1 nM) and in either male or female COC-doped LFPs (~60 μM). The latter corresponds to ~300 ng, which falls within the range reported for COC excreted through sweat. The method was also tested for its predominant metabolite, benzoylecgonine (BENZ), which exhibited a similar performance. Adsorption of analytes on AuNRs was investigated with the aid of different isotherm models. Freundlich and Frumkin models were the best and revealed that COC and BENZ are equally physiosorbed ($\Delta G^0_{ads} \sim -30$ kJ mol^{-1}) onto a heterogenous surface (AuNRs) with a discrete attractive interaction between adsorbed species. Considering that the photochemical synthesis is completed in about 30 min, and that staining of LFPs is easily done, photochemically-made AuNRs offer a relatively simple yet very sensitive method for assisting in COC detection.

Introduction

Cocaine (COC) falls under the category of alkaloids, which are organic compounds containing a nitrogen atom attached to a heterocyclic ring, imparting a basic nature to these substances.[1,2] It is a psychotropic drug that acts as a central nervous system stimulant and also exhibits analgesic properties.[2,3] Its recreational usage among individuals between 15 and 64 years old has been predominantly concentrated in the Americas, Oceania and Europe, with South America being recognized as the primary distribution hub for North America, Central America, and Western Europe.[4] COC is the major analyte excreted in sweat following its administration. Smaller amounts of benzoylecgonine (BENZ), which is a main, biologically active metabolite of COC can also be detected in body fluids of COC consumers.[5]

Several analytical approaches have been developed for the detection of COC in chemical and biological samples, including mass spectrometry,[6,7] fluorescence,[8] gas chromatography with flame ionization detection (GC-FID)[9] and gas chromatography-mass spectrometry (GC-MS).[10] However, they are costly, demand a long operation time, sample pre-treatment and trained operators. Many available field techniques, such as lateral flow immunoassays, can suffer from limited sensitivity or cross-reactivities.[8] These features can severely limit the reliable determination of COC and BENZ at a faster rate in real-world situations, for example, in latent fingerprints (LFP).

LFP is one of the most important types of evidence for crimes authorship. The fingerprint is composed of a mixture of endogenous (amino acids, lipids, proteins) and exogenous (drugs, cosmetics, explosives) components.[11] LFPs, by definition, lack visible contrast under normal lighting conditions and are, therefore, not perceptible to the naked eye. However, they can be visualized through physicochemical techniques, such as the application of revealing powders or the use of reagent vapours that interact with secretion components and produce sufficient contrast for detection.[12,13] Since the mid-1990s, fingerprint analysis methods have evolved,[14] especially with regard to the search for other information such as dating,[15] sex determination,[16,17] chemical imaging[18] and traces of substances that have been consumed or manipulated by suspect

[a]*Instituto Nacional de Identificação, Polícia Federal, 70770-917, Brasília-DF, Brazil. E-mail: desouza.mas@outlook.com*

[b]*Universidade de Brasília, Instituto de Química, Laboratório de Pesquisa em Polímeros e Nanomateriais, 70910-900, Brasília-DF, Brazil*

[c]*Universidade de Brasília, Faculdade de Ceilândia, Laboratório de Nanotecnologia Verde, 72220-900, Brasília-DF, Brazil*

[d]*Universidade de Brasília, Instituto de Química, Laboratório de Automação, Quimiometria e Química Ambiental, 70910-900, Brasília-DF, Brazil*

individuals.[7,19] Indeed, detection and identification of drug traces in LFP is a very convenient way for the forensic activity, as sampling and measuring can be performed in dried state.

On the other hand, SERS spectroscopy has shown potential not only in the detection and quantification of drugs of abuse, such as cocaine COC,[20–23] but also in the simultaneous acquisition of fingerprint images and their corresponding specific chemical information, which significantly broadens its forensic applications.[24] The technique is renowned for its exceptional sensitivity towards cocaine and its analogues, with literature reports demonstrating detection limits in the nanomolar (nM) range for these substances in various matrices.[20–23] Because of its high sensitivity and the possibility of using portable spectrometers, SERS spectroscopy can be performed rapidly and has great potential in forensic activities. It is full use relies on SERS active substrates. In general, these substrates can be made with a solid support, rigid or flexible (*e.g.* glass slides, paper, plastic *etc*), with adsorbed Ag and Au nanoparticles (Ag-NP and Au-NP).[25] The inherent localized surface-plasmon resonance (LSPR) of these nanoparticles intensifies the electromagnetic field in the vicinity of adsorbed molecules, which causes a signal enhancement of several orders of magnitude,[26] including the possibility of detecting a single molecule.[27] Besides that, this intensification may impair the influence of fluorescence background that usually accompanies such analysis and is responsible for a decrease of the Raman signal.

Despite the promising feature, a limited studies have demonstrated the possibility of SERS detection of illicit drugs in LFPs.[18,28–30] In this regard, herein we report the application of photochemically-made gold nanorods (AuNRs), with aspect ratio of 1.7, as SERS substrates for adsorption and detection of COC in LFP. The AuNRs were produced as a stable colloidal sample using a simple and eco-friendly UV-assisted method, which is completed in 30 min. It is observed that the optimal removal of CTAB, which is used as a shape agent, plays a pivotal role for the production of AuNRs displaying suitable SERS effect for detection of COC either in solution as well as in LFP. The SERS substrates demonstrate equivalent performance for BENZ. Three adsorption models were applied to adjust the isotherms and suggested that AuNRs have a heterogenous surface, where COC and BENZ are favorably adsorbed in a physical way.

Experimental

Reagents and materials

Hexadecyltrimethylammonium bromide (CTAB, 98%), chloroauric acid trihydrate ($HAuCl_4 \cdot 3H_2O$ 99%), silver nitrate ($AgNO_3$ 99%), acetone P. A., cyclohexane P. A., ascorbic acid (AA, 99%), and rhodamine 6G (R6G, 95%) were purchased from Sigma-Aldrich (USA) and used as received. Cocaine hydrochloride (COC) was provided by the Brazilian Federal Police, Brasilia-DF, Brazil. The purity of this sample, as determined by ^{1}H-NMR spectroscopy, was 88.27%. Certified BENZ (79.62%) was purchased from INMETRO (Brazil). All other chemicals used in the experiments were of analytical grade and used as received as well. The preparation of solutions and cleaning of glassware were done with ultrapure water, resistivity 18 MΩ cm provided by a Millipore Mili-Q Direct8 system. One-inch square, polished aluminum slides were employed as substrates for SERS measurements (solution and LFP).

Photochemical synthesis of AuNRs

The synthesis protocol followed that previously reported by Abdelrasoul *et al.*[31] with minor modifications. In a typical run as depicted in Scheme 1A, a borosilicate glass beaker (25 mL), which was previously cleaned with *aqua regia* solution (HCl : HNO_3, 3 : 1, v/v) and rinsed several times with ultrapure water, was filled with 7.2 mL of CTAB solution (2.4×10^{-4} g L^{-1} or 0.54 μM), 2.0 mL of $HAuCl_4$ (3 g L^{-1} or 7.6 mM), 178 μL of $AgNO_3$, (2 g L^{-1} or 11.7 mM), 195 μL of acetone and 135 μL of cyclohexane, in this order. After each added material, the mixture was stirred and displayed a vivid orange color at the end, typical of Au^{3+} species. Next, 80 μL of AA (0.1 g L^{-1} or 0.57 mM) were added and the mixture became colorless, indicating the reduction of Au^{3+} to Au^{1+}.[31] The beaker with the colorless mixture was then transferred to the UV chamber, Scheme 1B, being positioned 5 cm below the lamps and submitted to UV irradiation for 30 min under room temperature. The UV chamber, Scheme 1B, is made of stainless steel and equipped with six UV lamps (8 W, 254 nm, Osram), an Arduino Uno R3 microcontroller and a touch screen display, the latter capable of displaying the light power and dosage and time of light exposition. The irradiance and fluence were previously calibrated with a certified power meter (Instrutherm MRU-201, Brazil). For the synthesis of AuNRs, the radiation intensity was set at 12.1 mW cm^2 and fluence at 21.8 J cm^2. Under radiation intensities lower than that, no nanorods could be formed. After this time, the reaction displayed a mix of blue and brown tones, which are assigned to AuNRs and other shapes of Au nanoparticles. The product was purified after successive washing cycles with ultrapure water and centrifugation at 13 375*g* for 20 min. each. The products obtained were resuspended in 2.0 mL of ultrapure water in Eppendorf tubes and named NR1, NR2, NR3, and NR4, according to the number of purification cycles, 1, 2, 3, or 4, respectively. A digital photograph of these samples is shown in Scheme 1C.

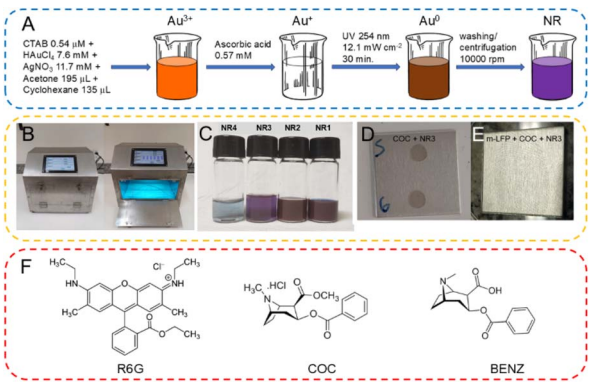

Scheme 1 Illustration of the (A) photochemical synthesis of AuNRs, (B) UV chamber, (C) products after washing/centrifugation cycles, (D) COC + NR3 and (E) m-LFP + COC + NR3 samples for SERS measurements, and (F) chemical structures of R6G, COC, and BENZ.

Characterization of AuNRs

The absorption spectrum of colloidal AuNRs samples was obtained with a Shimadzu UV-Vis 2450 spectrophotometer within the range of 200−800 nm, at 10 nm s^{-1} scan rate, and resolution of 0.1 nm. Hydrodynamic size and zeta potential were simultaneously determined by dynamic and electrophoretic light scattering (DLS/ELS) measurements using a Malvern Zeta Sizer ZS90 instrument. Transmission electron microscopy (TEM) images were obtained using a JEOL JEM-2100 microscope at 200 keV. Images were quantitatively analyzed using the ImageJ software. The *d*-spacing was estimated by applying fast Fourier transform to the images of individual nanoparticles and counting of the interference fringes. The mean dimensions of the nanorods, length (L) and width (W), were determined from a size distribution histogram built with the diameters of 300 particles collected from several images. The histogram was built according to the Sturge's rule,[32] which defines that the number of bins or classes (C) scales with the number of particles (N), according to eqn (1):

$$C = 1 + 3.322x \log N \quad (1)$$

Preparation of samples, SERS measurements and adsorption studies

Raman and SERS measurements were performed with a Renishaw InVia Raman microscope equipped with a thermoelectric cooled CCD detector, 1200 lines per groove diffraction grating and two laser lines: 632.8 nm (HeNe) and 785 nm (diode laser). The laser beam was focused on the sample using a Leica microscope with a 50× objective lens. The nominal spectral resolution was 6 cm^{-1}. The wavenumbers were calibrated with the signal of Si wafer at 520 cm^{-1}. All SERS spectra were recorded using the 785 nm diode laser line at a laser power of 30 mW (measured at the entrance of the instrument, just before the gray filter wheel).

Stock solutions of the analytes, namely R6G, COC and BENZ (Scheme 1F) were prepared by dissolving a proper mass of each substance in ultrapure water assisted by magnetic stirring. After that, the samples were properly diluted with ultrapure water in borosilicate volumetric flasks in the following concentrations ranges: 1×10^{-6} to 3×10^{-12} M (R6G), 5.0×10^{-2} to 1.0×10^{-9} M (COC), and 1.0×10^{-2} to 8.0×10^{-8} M (BENZ).

The aluminum slides where samples were adsorbed and measured were sequentially cleaned with alkaline solution (70% (v/v) NH_4OH and 30% (v/v) H_2O_2), "piranha" solution (70% (v/v) concentrated H_2SO_4 and 30% (v/v) H_2O_2), and ultrapure water. The slides were then blow dried with compressed air.

The samples for SERS measurements were prepared in 1.0 mL Eppendorf tubes by mixing 15 μL of the analyte at the desired concentration and 15 μL of the AuNRs colloidal suspension. The homogenous mixture was then dropped on the cleaned aluminum slide and left drying for 24 h in the air. Scheme 1D shows a digital photography of a representative sample. This procedure was adopted for standardization and mapping. For an on-site analysis, however, its time can be shortened, for example, by using pre-synthesized AuNRs and accelerating drying of the slides with an air blower.

All SERS spectra were registered at room temperature (25 °C). The spectra were acquired from different sample spots, in intervals of 2 μm covering an area of 20 μm × 20 μm using the 50× objective. Each spectrum was registered after averaging the signal over 3 s of integration time. For each concentration, an average of 100 spectra was accounted.

Adsorption isotherms were built with the surface coverage (θ) of the aluminum substrate as a function of the equilibrium concentration (c_{eq}) of R6G, COC and BENZ. θ was calculated using eqn (2):

$$\theta = \frac{q_e}{q_{max}} = \frac{I}{I_0} \quad (2)$$

in which, q_e and q_{max} stand for the amount adsorbed at equilibrium and that needed for total surface coverage, respectively. For the current experiment, they were correlated to the SERS signal intensity where I is the SERS intensity of the analyte at any particular adsorbate solution concentration, and I_0 is the SERS intensity of the same band at the saturation concentration, respectively. For R6G, the intensity was measured at 612 cm^{-1} (xanthene ring deformation), while for COC and BENZ the intensity was measured at 1001–1004 cm^{-1} (aromatic ring breathing). Langmuir, Freundlich and Frumkin models, according to eqn (3)–(5), were used to adjust the experimental data using the Origin Pro 8.5 software.

$$\theta = \frac{Kc_{eq}}{1 + Kc_{eq}} \quad (3)$$

$$\theta = K' c^{\frac{1}{n}} \quad (4)$$

$$\theta = \frac{Kc_{eq}{}^{g}}{1 + Kc_{eq}{}^{g}} \quad (5)$$

In eqn (2), K is the Langmuir constant (equilibrium constant), and c_{eq} is the equilibrium concentration of adsorbate (bulk solution concentration).[32] In eqn (3), K' and n are simply adjustment constants for a given adsorbate and adsorbent at a given temperature.[33] In eqn (4), g ($= -2\omega/RT$) is a parameter usually associated to the presence of attractive (also called lateral interaction), $g > 0$, or repulsive interactions, $g < 0$, between adsorbed species.[34]

The preparation and SERS measurements of COC samples on fingerprints followed the procedures described below. LFPs of two volunteers were used, a male (m-LFP) and a female (f-LFP), both Caucasians, aged 46 and 45 years, respectively. The volunteer rubbed the right finger thumb against his/her forehead for 3 s in order to grease it. The finger thumb was then contacted for 5 s to a clean aluminum slide containing 50 μL of COC (50 mM, 10 mM, and 0.6 mM). Then, the NR3 colloid was cast on the LFP and left it drying for 24 h at room temperature. Scheme 1E shows a typical fingerprint sample. Raman spectra were acquired using the mapping function in three different regions of the LFP stained with NR3. The spectrum of each region was obtained after averaging 100 spectra, which were registered according to the procedure above described.

Results and discussion

Structure and morphology of AuNRs

A summary of the structural/morphological characteristics of sample NR3 is displayed in Fig. 1. NR3 was chosen because as we shall see in the next sections, it shows the best SERS activity. The UV-Vis spectrum of NR3 is shown in Fig. 1A (in black) and features two electronic transitions, one at 524 nm and other at 617 nm, which are ascribed to the transversal and longitudinal LSPR modes in AuNRs, respectively.[35] The separation between peaks has a straightforward correlation with the particles' aspect ratio (L/W).[35] Still in Fig. 1A, the sample's spectra registered during 28 days of aging (stored inside a drawer, in the dark and at room temperature) have only the longitudinal LSPR mode changed, with a blue-shift of 12 nm that can be related to aggregation of particles. Nonetheless, this change occurs only between day 1 and day 2, and from then on, the spectrum remains practically unaltered. This is confirmed by the graph inserted in Fig. 1A, which shows the dependence of the absorbance ratio of the two bands (A_{605}/A_{524}) on the day of measurement. This ratio levels-off at approximately 1.23, meaning that the shape of particles is fairly stable.

A typical TEM image of NR3, Fig. 1B, shows nanorods of rounded corners as the prevalent shape, but with variable L and W (*i.e.* polydisperse). The high-resolution image displayed in Fig. 1C shows in detail the crystalline planes, with a regular distance of 0.24 nm. When using the Bragg equation for the cubic system, this value equals to the d-spacing for (111) planes in FCC gold. Additionally, Fig. 1D shows the SAED pattern indexed in agreement with the Au JCPDS file: 04-0784. Fig. 1E and F display the size histograms of L and W of the nanorods, whose mean values were determined by the log-normal fitting as 76.3 ± 2.11 nm and 44.32 ± 5.34 nm, respectively. This gives an aspect ratio of 1.72. For reference, Abdelrasoul *et al.*[31] using a UV-assisted method obtained nanorods of aspect ratio ranging from ~3.2 to 4.5 when the irradiance was increased from 1.3 mW cm^{-2} to 6.6 mW cm^{-2}. Herein, we applied 12.1 mW cm^2 and fluence of 21.8 J cm^2, since under radiation intensities lower than that, no nanorods could be formed at all. It can be speculated that in our synthesis, the growth prevails over the nucleation step, leading to wider nanorods. Additionally, DLS/ELS measurements (Table S1) show that NR samples display a hydrodynamic size ranging between 45.5 nm and 37.2 nm and zeta potential ranging from + 39.5 mV to + 30.6 mV, when increasing the number of washing/centrifugation cycles from 1 to 4.

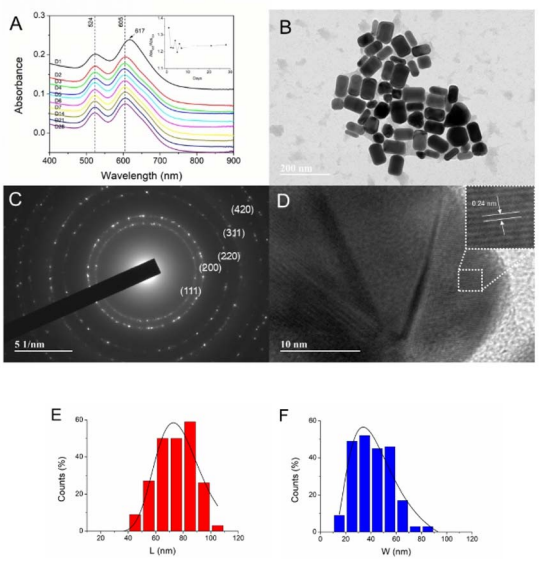

Fig. 1 Structural and morphological characteristics of the NR3 sample: (A) UV-Vis spectra registered in the day of synthesis and during subsequent days (until 28). The inset shows the change on the ratio of absorbances measured at 605 nm and 524 nm with the day of measurement. (B) Low and (C) high-resolution TEM images. The inset in (C) gives a zoomed view of the tip of a nanorod and highlights the d-spacing. (D) SAED showing the plane indexes. (E) Length (L) and (F) width (W) distribution of the nanorods.

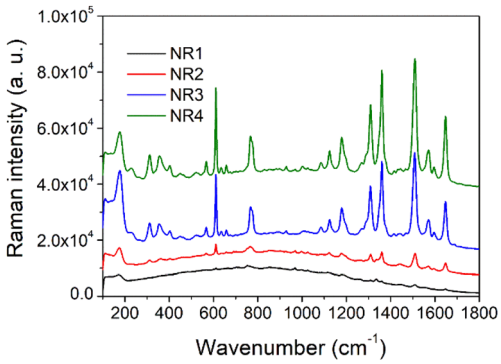

Fig. 2 SERS spectra of R6G (50 nM) adsorbed on NR1, NR2, NR3, and NR4, as indicated.

Optimization of Au-NR sample for SERS application

The reaction mixture for production of AuNRs is roughly described by an equilibrium between AuNRs coated with a compact CTAB bilayer structure (~3 nm thick), micelles, and surfactant monomers.[36] The excess of CTAB must be, therefore, removed to improve the contact (or decrease the distance) of analytes with the plasmonic nanoparticles. Considering that aspect, we first evaluated the SERS activity of these NR samples with R6G, which is a well-stablished SERS probe.

SERS spectra of R6G (50 nM) adsorbed on NR1, NR2, NR3, and NR4 are collected in Fig. 2. The spectra are typical of R6G, as discussed in the next paragraph, and look better resolved as

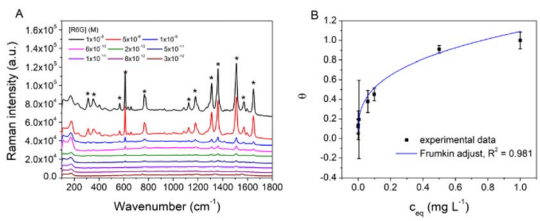

Fig. 3 (A) SERS spectra of R6G (1×10^{-8} to 3×10^{-12} M) adsorbed onto NR3. (B) Isotherms for adsorption of R6G on NR3.

Table 1 Fitting parameters for the adsorption of R6G on NR3

Model	R^2	K/L mg^{-1} (M^{-1})	n	g	$-\Delta G^0_{ads}$/kJ mol^{-1}
Langmuir	0.944	11.66 (2.43×10^5)	—	—	38.4
Freundlich	0.981	1.9	3.73	—	—
Frumkin	0.981	0.545 (8.8×10^6)	—	0.325	33.9

more washing/centrifugation cycles are performed. This result corroborates with our standing hypothesis. Moreover, a comparison between spectra attained with NR3 and NR4 does not show significant differences either in terms of intensity or resolution. It has been observed, however, that the amount of AuNRs decreases considerably with each purification cycle, specially from NR3 to NR4, as noted by the photographs of Scheme 1C. Therefore, as mentioned in the previous section, sample NR3 was chosen for the subsequent studies.

Fig. 3A displays SERS spectra for R6G, ranging from 1×10^{-8} to 3×10^{-12} M, adsorbed onto NR3. The band assignment is listed in Table S2, where the main ones located at 610 cm^{-1}, 1361 cm^{-1}, and 1510 cm^{-1}, are ascribed to deformation and stretching of the xanthene ring as reported elsewhere.[37] It is worth mentioning that the xanthene ring deformation band at 610 cm^{-1} is still detectable in the spectrum even at 5×10^{-11} M. The adsorption isotherm based on the intensity of this band is shown in Fig. 3B. It has an asymptotic shape, with a saturation plateau starting at ~0.5 mg L^{-1}.

Three different adsorption models were tested to adjust these experimental data: Langmuir, Freundlich and Frumkin (eqn (3)–(5)). Table 1 shows the respective fitting parameters. Although all the three models can fit the experimental data, Freundlich and Frumkin models do it at best (highest R^2). Accordingly, NR3 displays a heterogeneous surface, as the adsorption of R6G fits well within the Freundlich model. Also, the adsorption is favoured, as the exponent n extracted from fitting is larger than 1.[33] Additionally, as $g > 0$ (=0.325) in the Frumkin equation, it suggests an attractive interaction between adsorbed species. This is expected since R6G molecules are known to aggregate in aqueous media.[38]

The free-energy of adsorption (ΔG^0_{ads}) was estimated using K from Langmuir and Frumkin models, which gave close values, −38.4 kJ mol^{-1} and -33.9 kJ mol^{-1}, respectively. They are typical of physisorption.[39] Values of K, g, and ΔG^0_{ads} are comparable to those reported for the adsorption of R6G onto spherical Ag nanoparticles.[40]

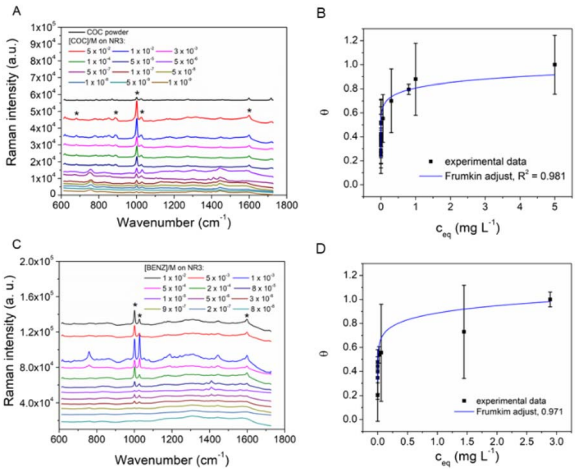

Fig. 4 COC and BENZ adsorption on NR3. SERS spectra of (A) COC and (B) BENZ (1 nM to 50 mM) adsorbed on NR3, and respective adsorption isotherms, (C) and (D).

These findings reveal that the washing/centrifugation step is crucial to control the SERS activity of the NR substrate. Since the zeta potential of NR samples has marginally changed with purification (Table S1), only empty micelles and free monomer should be removed. As reported elsewhere, CTAB interacts strongly with R6G.[41] This condition decreases their availability to interact more directly with AuNRs, thus resulting in a less efficient SERS effect. Additionally, eventual electrostatic repulsion occurring between the CTAB bilayer coating AuNRs and R6G molecules seems to not play a pivotal role in the SERS effect. This information is especially important for the SERS detection of street cocaine (cocaine hydrochloride), which has cationic molecules.

Adsorption and SERS detection of COC and BENZ on the NR3 substrate

Fig. 4 collects SERS spectra of COC and BENZ at different concentrations (1 nM to 50 mM) in the presence of the NR3 substrate. In Fig. 4A, the spectra display the main signal of COC, which is the aromatic ring breathing mode peaking at 1001–1007 cm^{-1}. For comparison purposes, Fig. S1 provides the Raman spectrum of powder COC from which samples were prepared for the study. The main bands of Raman and SERS spectra were tentatively assigned according to the literature[42–45]

Table 2 Fitting parameters for the adsorption of COC and BENZ on NR3

Model	R^2	K/L mg^{-1} (M^{-1})	n	g	$-\Delta G^0_{ads}$/kJ mol^{-1}
COC					
Freundlich	0.988	0.806	12.78	—	—
Frumkin	0.981	0.403 (1.37×10^5)	—	0.0785	29.3
BENZ					
Freundlich	0.941	1.525	10.45	—	—
Frumkin	0.971	0.443 (1.28×10^5)	—	0.0957	29.1

and are collected in Table S3. Comparatively, in the same figure, the SERS spectrum of COC at 50 μM retains only part of these bands, as seen for the lower COC concentrations as well. Some bands shift position; the smallest shifts were about 1 cm^{-1} to 3 cm^{-1}, while the largest were 9 cm^{-1} and 18 cm^{-1}. It is worth mentioning that the largest shifts were found in the C–C stretching in the tropane ring. The polarizability of this bond is affected by the presence of protonated nitrogen.[45] BENZ spectra have similar features, with emphasis on the aromatic ring breathing mode, observed at 1001 cm^{-1}. In addition, the C–N stretching at 1026 cm^{-1} is much more prominent than in COC spectra, sometimes being equivalent or more intense than the aromatic ring breathing mode (see spectra at 1.0 mM, 0.5 mM, and 10 μM). This may be caused by the carboxylic acid group that is formed upon metabolization of COC into BENZ (Scheme 1F).

Just like R6G, adsorption of COC and BENZ on NR3 follows an asymptotic fashion, in which a saturation plateau starts at ~0.5 mg L^{-1}, as shown in Fig. 4B and D. We attempted to fit data with the same three isotherm models, but only two (Freundlich and Frumkin) worked well for these substances, as displayed in Table 2. The respective fitting parameters indicate that adsorption of COC and BENZ occurs on a heterogeneous surface (AuNRs) and is spontaneous. Some attractive interaction between adsorbing species is detected, as $g > 0$ for the adsorption of both species. Nonetheless, this aspect is less pronounced than in the adsorption of R6G. In summary, the difference between COC and BENZ molecular structures does not influence their adsorption characteristics at a detectable rate. More specifically, ΔG^0_{ads} determined for COC is −29.3 kJ mol^{-1}, while for BENZ is −29.1 kJ mol^{-1}. These values are comparable to those found elsewhere for adsorption of COC; for instance, −28.96 kJ mol^{-1},[46] −61.5 kJ mol^{-1}.[47] A value of −24 kJ mol^{-1} has been reported for the adsorption of methamphetamine on Ag nanoparticles.[29] It should be pointed out that these adsorption models show limitations. The principal limitation of the Langmuir model arises from its assumption of a homogeneous adsorption surface and the neglect of interactions among adsorbed species, assumptions that seldom hold under practical conditions. In contrast, the Frumkin model incorporates lateral interactions; however, its characteristic interaction parameter often exhibits instability, and the model's inherent complexity can impede consistent and reliable interpretation, particularly in heterogeneous or multi-component systems.

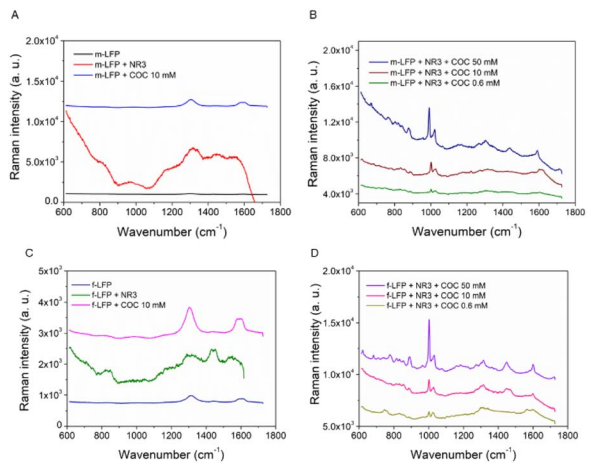

Fig. 5 SERS detection of COC on male and female LFPs. Spectra of (A) male and (C) female LFP (plain, in the presence of NR3 and COC (10 mM)). Spectra of (B) male and (D) female LFP contaminated with COC (0.6 mM, 10 mM, and 50 mM), in the presence of NR3, as indicated.

COC detection in fingerprints

The successful detection of COC in LFPs using the NR3 substrate, characterized by the adsorption studies, confirms that the physisorption process remains effective even when the analyte is pre-deposited within the complex fingerprint matrix, validating the relevance of the isotherm models for this practical application. SERS detection of COC in LFPs of male and female volunteers was evaluated with samples prepared as described in the experimental section. As shown in Fig. 5A and C, the plain m-LFP shows no detectable Raman signal while the f-LFP displays a single peak at 1311 cm^{-1}. This wavenumber can be ascribed to the C–H twisting in hydrocarbon chains from fatty acids found in the skin secretions.[48] Upon addition of COC at 10 mM, only the signal at 1311 cm^{-1} is seen in the spectra of both samples, which is more enhanced in the m-LFP. This is because the Raman spectrum of COC also displays this band, thus summing up with that inherent to the plain LFP. On the other hand, as shown in Fig. 5B and D, spectra of COC-doped LFPs registered in the presence of NR3 show the typical signature of COC, regardless the sample is from a male or female volunteer. It is worth noting that even for the lowest COC concentration added to the LFP, 60 μM, it is possible to detect COC, because of the signal at 1004 cm^{-1} which is still observed. Indeed, a rougher estimation considering the measurement area gives a trace amount of 273 ng of COC. This value falls within the range reported for cocaine excreted through sweat (33 a 3579 ng per patch).[49] Moreover, the photochemical method is simpler, faster, and more energy-efficient, making it a promising approach for the effective production of SERS-active nanoparticles.

Conclusions

It has been shown that rod-shaped gold nanoparticles (AuNRs) can be easily produced by UV-assisted reduction of $HAuCl_4$ in the presence of CTAB. A succession of two washing/centrifugation cycles is sufficient to remove the excess of CTAB and produce AuNRs displaying suitable SERS effect for detection of cocaine hydrochloride (COC), in solution as well as in latent fingerprints. They can also be applied for detection of COC metabolite, benzoylecgonine (BENZ). Adsorption models applied to isotherms suggest that AuNRs exhibit a heterogenous surface where COC is physiosorbed, probably permeating within the CTAB bilayer. A similar behavior was observed for BENZ, despite its slightly different chemical structure. The AuNRs enabled SERS detection of COC at 1 nM when spread onto aluminum substrates and 60 μM in latent fingerprints. The

latter corresponds to 275 ng of COC, which is a trace amount and made detectable thanks to the SERS effect promoted by AuNRs. Considering that this method for production of AuNRs is relatively simple, validation in routine forensic analysis should demonstrate its potential for detection of cocaine and other drugs of abuse. Future work will include a direct comparative study with benchmark SERS substrates to further contextualize the performance of these photochemically-synthesized AuNRs.

Author contributions

M. A. Souza: conceptualization, investigation, methodology, data curation, writing – review & editing. K. V. de Oliveira: investigation, data curation. L. B. Pereira: investigation, data curation. M. H. Sousa: supervision, writing – review & editing, fund acquisition. J. W. B. Braga: supervision, writing – review & editing. L. G. Paterno: conceptualization, supervision, writing – review & editing, fund acquisition.

Conflicts of interest

There are no conflicts to declare.

Ethical statement

The Ethics and Human Research Committee of the Faculty of Health Sciences of the University of Brasília approved this research (protocol 42304220.0.0000.0030), in accordance with resolution 466/12 of the National Health Council (CNS). Written informed consent was obtained from all volunteers prior to their participation.

Data availability

Raw fingerprint images and related metadata collected from human participants are not publicly available due to confidentiality agreements approved by the institutional ethics board.

All data supporting the findings of this study are available in the main text and supplementary information (SI). Supplementary information is available. See DOI: **https://doi.org/10.1039/d5ra04284d**.

Acknowledgements

The authors acknowledge the financial support of CAPES (financial code 001), CNPq, FAP-DF (grant numbers: 00193.00001824/2022-64). Authors also acknowledge the technical support of Dra. Tatiane O. dos Santos from the Multiuser Laboratory for High-Resolution Microscopy (LABMIC-UFG) for the TEM measurements and Dr Adriano O. Maldaner from the Brazilian National Institute of Criminalistics of Federal Police (INC-PF) for gently providing the benzoylecgonine sample.

Notes and references

1 M. F. Roberts and M. Wink, in *Alkaloids: Biochemistry, Ecology, and Medicinal Applications*, Springer US, Boston, 1998.
2 S. Bhambhani, K. R. Kondhare and A. P. Giri, Diversity in Chemical Structures and Biological Properties of Plant Alkaloids, *Molecules*, 2021, **26**, 3374.
3 A. Cecinato, C. Balducci and M. Perilli, Illicit Psychotropic Substances in the Air: The State-of-Art, *Sci. Total Environ.*, 2016, **539**, 1–6.
4 United Nations Office on Drugs and Crime, *Global Report on Cocaine 2023 – Local Dynamics, Global Challenges*, United Nations Publications, 2023.
5 E. J. Cone, M. J. Hillsgrove, A. J. Jenkins, R. M. Keenan and W. D. Darwinet, Sweat Testing for Heroin, Cocaine, and Metabolites, *J. Anal. Toxicol.*, 1994, **18**, 298–305.
6 C. Costa, R. Webb, V. Palitsin, M. Ismail, M. de Puit, S. Atkinson and M. J. Bailey, Rapid, Secure Drug Testing Using Fingerprint Development and Paper Spray Mass Spectrometry, *Clin. Chem.*, 2017, **63**, 1745–1752.
7 M. Jang, C. Costa, J. Bunch, B. Gibson, M. Ismail, V. Palitsin, R. Webb, M. Hudson and M. J. Bailey, On the Relevance of Cocaine Detection in a Fingerprint, *Sci. Rep.*, 2020, **10**, 1974.
8 Y. Zhang, Z. Sun, L. Tang, H. Zhang and G.-J. Zhang, Aptamer Based Fluorescent Cocaine Assay Based on the Use of Graphene Oxide and Exonuclease III-Assisted Signal Amplification, *Microchim. Acta*, 2016, **183**, 2791–2797.
9 Y. Zuo, K. Zhang, J. Wu, C. Rego and J. Fritz, An Accurate and Nondestructive GC Method for Determination of Cocaine on US Paper Currency, *J. Sep. Sci.*, 2008, **31**, 2444–2450.
10 V. S. Menotti, *et al.*, Validation of a Method for Simultaneous Analysis of Cocaine, Benzoylecognine and Cocaethylene in Urine using Gas Chromatography-Mass Spectrometry, *Braz. J. Pharm. Sci.*, 2020, **56**, e18664.
11 R. S. Croxton, S. M. Bleay and M. De Puit, Composition and Properties of Fingermarks, in *Fingerprint Development Techniques: Theory and Application*, John Wiley & Sons Ltd, 1st edn, 2018, pp. 35–68.
12 F. M. Gomes, C. M. P. de Pereira, K. de Cássia Mariotti, T. M. Pereira, N. A. dos Santos and W. Romão, Study of Latent Fingerprints – A Review, *Forensic Chem.*, 2023, **35**, 100525.
13 G. Martins, R. M. Barros, M. P. de Sousa, K. P. M. Frin, M. A. de Souza and L. G. Paterno, Fluorescent Carbon Dots for Improved Visualization of Latent Fingermarks after Cyanoacrylate Fuming, *ACS Appl. Nano Mater.*, 2024, **7**, 25891–25899.
14 R. Delorenzo and D. R. Kimbrough, Solving the Mystery of the Fading Fingerprints with London Dispersion Forces, *J. Chem. Educ.*, 1998, **75**, 1300.
15 H. Chen, M. Shi, R. Ma and M. Zhang, Advances in Fingermark Age Determination Techniques, *Analyst*, 2021, **146**, 33–47.
16 M. A. Souza, A. S. Santos, S. W. da Silva, J. W. B. Braga and M. H. Sousa, Raman Spectroscopy of Fingerprints and

Chemometric Analysis for Forensic Sex Determination in Humans, *Forensic Chem.*, 2022, **27**, 100395.
17 D. S. Carvalho, M. M. V. de Alecrim, R. T. de Sousa Júnior and L. A. Ribeiro Júnior, Outcome of Sex Determination from Ulnar and Radial Ridge Densities of Brazilians' Fingerprints: Applying an Existing Method to a New Population, *Sci. Justice*, 2022, **62**, 181–192.
18 R. M. Connatser, S. M. Prokes, O. J. Glembocki, R. L. Schuler, C. W. Gardner, S. A. Lewis Sr and L. A. Lewis, Toward Surface-Enhanced Raman Imaging of Latent Fingerprints, *J. Forensic Sci.*, 2010, **55**, 1462–1470.
19 A. Bécue and C. Champod, Interpol review of fingermarks and other body impressions 2019–2022, *Forensic Sci. Int.: Synergy*, 2023, **6**, 100304.
20 B. Yu, M. Ge, P. Li, Q. Xie and L. Yang, Development of Surface-Enhanced Raman Spectroscopy Application for Determination of Illicit Drugs: Towards a Practical Sensor, *Talanta*, 2019, **191**, 1–10.
21 J. T. Zhao, C. Y. Xu, Y. B. Duan, P. X. Zhang, M. Z. Si and Q. Yang, Raman Investigating of Trace Contraband Heroin by Micro Raman Spectroscopy, *Spectral Anal.*, 2002, **22**, 588–590.
22 C. Andreou, M. R. Hoonejani, M. R. Barmi, M. Moskovits and C. D. Meinhart, Rapid Detection of Drugs of Abuse in Saliva Using Surface Enhanced Raman Spectroscopy and Microfluidics, *ACS Nano*, 2013, **7**, 7157–7164.
23 R. Elashnikov, O. Khrystonko, A. Trelin, M. Kuchař, V. Švorčík and O. Lyutakov, Label-Free SERS-ML Detection of Cocaine Trace in Human Blood Plasma, *J. Hazard. Mater.*, 2024, **472**, 134525.
24 T. Zhang, *et al.*, Surface-enhanced Raman imaging through sprayed probes for the application in chemical visualization of methamphetamine within fingerprints, *Anal. Bioanal. Chem.*, 2023, **19**, 4713–4723.
25 K. Kant, *et al.*, Roadmap for Plasmonic Nanoparticle Sensors: Current Progress, Challenges and Future Prospects, *Nanoscale Horiz.*, 2024, **9**, 2085–2166.
26 K. A. Willets and R. P. Van Duyne, Localized Surface Plasmon Resonance Spectroscopy and Sensing, *Annu. Rev. Phys. Chem.*, 2007, **58**, 267–297.
27 K. Kneipp, Y. Wang, H. Kneipp, L. T. Perelman, I. Itzkan, R. R. Dasari and M. S. Feld, Single Molecule Detection Using Surface-Enhanced Raman Scattering (SERS), *Phys. Rev. Lett.*, 1997, **78**, 1667.
28 T. Yang, X. Guo, H. Wang, S. Fu, Y. Wen and H. Yang, Magnetically Optimized SERS Assay for Rapid Detection of Trace Drug-Related Biomarkers in Saliva and Fingerprints, *Biosens. Bioelectron.*, 2015, **68**, 350–357.
29 M. A. Souza, K. V. de Oliveira, F. C. C. Oliveira, L. P. Silva and J. C. Rubim, The Adsorption of Methamphetamine on Ag Nanoparticles Dispersed in Agarose Gel - Detection of Methamphetamine in Fingerprints by SERS, *Vib. Spectrosc.*, 2018, **98**, 152–157.
30 J. S. Day, H. G. M. Edwards, S. A. Dobrowski and A. M. Voice, The Detection of Drugs of Abuse in Fingerprints Using Raman Spectroscopy I: Latent Fingerprints, *Spectrochim. Acta, Part A*, 2004, **60**, 563–568.
31 G. N. Abdelrasoul, R. Cingolani, A. Diaspro, A. Athanassiou and F. Pignatelli, Photochemical Synthesis: Effect of UV Irradiation on Gold Nanorods Morphology, *J. Photochem. Photobiol., A*, 2014, **275**, 7–11.
32 D. W. Scott, Sturge's Rule, *Wiley Interdiscip. Rev. Comput. Stat.*, 2009, **1**, 303–306.
33 A. W. Adamson and A. P. Gast, in *Physical Chemistry of Surfaces*, Wiley, 6th edn, 1997, p 808.
34 A. Frumkin, Die Kapillarkurve der Höheren Fettsäuren und Die Zustandsgleichung der Oberflächenschicht, *Z. Phys. Chem.*, 1925, **116**, 466–484.
35 S. Link and M. A. El-Sayed, Simulation of the Optical Absorption Spectra of Gold Nanorods as a Function of their Aspect Ratio and the Effect of the Medium Dielectric Constant. J. Phys. Chemistry B (1999) 103B, *J. Phys. Chem. B*, 2005, **109**, 10531–10532.
36 S. Gómez-Graña, F. Hubert, F. Testard, A. Guerrero-Martínez, I. Grillo, L. M. Liz-Marzán and O. Spalla, Surfactant (Bi)Layers on Gold Nanorod, *Langmuir*, 2012, **28**, 1453–1459.
37 M. Majoube and M. Henry, Fourier Transform Raman and Infrared and Surface-Enhanced Raman Spectra for Rhodamine 6G, *Spectrochim. Acta*, 1991, **4**, 1459–1466.
38 M. M. Wong and Z. A. Schelly, Solvent-Jump Relaxation Kinetics of the Association of Rhodamine Type Laser Dyes, *J. Phys. Chem.*, 1974, **78**, 1891–1895.
39 P. Atkins and J. de Paula, in *Atkins Physical Chemistry*, Oxford University Press, 8th edn, 2006, p. 917.
40 K. V. de Oliveira and J. C. Rubim, Surface-enhanced Raman Spectroscopy of Molecules Adsorbed on Silver Nanoparticles Dispersed an Agarose Gel and their Adsorption Isotherms, *Vib. Spectrosc.*, 2016, **86**, 290–301.
41 S. K. Maurya, D. Yadav and D. Goswami, Investigating Two-Photon-Induced Fluorescence in Rhodamine-6G in Presence of Cetyl-Trimethyl-Ammonium-Bromide, *J. Fluoresc.*, 2016, **26**, 1573–1577.
42 E. M. A. Ali, H. G. M. Edwards, M. D. Hargreaves and I. J. Scowen, Raman Spectroscopic Investigation of Cocaine Hydrochloride on Human Nail in a Forensic Context, *Anal. Bioanal. Chem.*, 2008, **390**, 1159–1166.
43 F. Inscore, C. Shende, A. Sengupta, H. Huang and S. Farquharson, Detection of Drugs of Abuse in Saliva by Surface-Enhanced Raman Spectroscopy (SERS), *Appl. Spectrosc.*, 2011, **65**, 1004–1008.
44 S. Farquharson, C. Brouillette, W. Smith and C. Shende, A Surface-Enhanced Raman Spectral Library of Important Drugs Associated with Point-of-Care and Field Applications, *Front. Chem.*, 2019, **7**, 706.
45 C. A. F. O. Penido, M. T. T. Pacheco, I. K. Lednev and L. Silveira, Raman Spectroscopy in Forensic Analysis: Identification of Cocaine and Other Illegal Drugs of Abuse, *J. Raman Spectrosc.*, 2016, **47**, 28–38.
46 R. Baweja, T. D. Sokoloski and P. N. Patil, Competitive Binding Between Cocaine and Various Drugs to Synthetic Levodopa Melanin, *J. Pharm. Sci.*, 1977, **66**, 1544–1547.

47 L. Pötsch, G. Skopp and G. Rippin, A comparison of 3H-cocaine binding on melanin granules and human hair in vitro, *Int. J. Leg. Med.*, 1997, **110**, 55–62.
48 T. R. Hata, T. A. Scholz, L. K. Pershing, I. V. Ermakov, R. W. McClane, F. Khachik and W. Gellermann, Non-invasive Raman Spectroscopic Detection of Carotenoids in Human Skin, *J. Invest. Dermatol.*, 2000, **115**, 441–448.
49 E. J. Cone, M. J. Hillsgrove, A. J. Jenkins, R. M. Keenan and W. D. Darwin, Sweat Testing for Heroin, Cocaine, and Metabolites, *J. Anal. Tox.*, 1994, **18**, 298–305.